Rotating Anisotropic Crystalline Silicon Nanoclusters in Graphene

Qu Chen,[†] Ai Leen Koh,[‡] Alex W. Robertson,[†] Kuang He,[†] Sungwoo Lee,[§] Euijoon Yoon,[§] Gun-Do Lee,[§] Robert Sinclair,[∥] and Jamie H. Warner*[,†]

[†]Department of Materials, University of Oxford, Parks Road, Oxford OX1 3PH, U.K., [‡]Stanford Nano Shared Facilities, Stanford University, Stanford, California 94305-4045, United States, [§]Department of Materials Science and Engineering, Seoul National University, Seoul 151-742, Republic of Korea, and [∥]Department of Materials Science and Engineering, Stanford University, Stanford, California 94305-4034, United States

ABSTRACT The atomic structure and dynamics of silicon nanoclusters covalently bonded to graphene are studied using aberration-corrected transmission electron microscopy. We show that as the cluster size increases to 4−10 atoms, ordered crystalline cubic phases start to emerge. Anisotropic crystals are formed due to higher stability of the Si−C bond under electron beam irradiation compared to the Si−Si bond. Dynamics of the anisotropic crystalline Si nanoclusters reveal that they can rotate perpendicular to the graphene plane, with oscillations between the two geometric configurations driven by local volume constraints. These results provide important insights into the crystalline phases of clusters of inorganic dopants in graphene at the intermediate size range between isolated single atoms and larger bulk 2D forms.

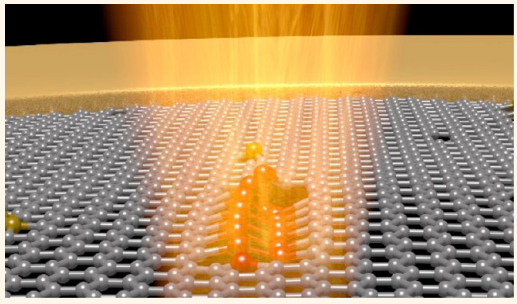

KEYWORDS: graphene · TEM · dopants · Si · atoms

Introducing foreign dopant atoms to pristine graphene provides an opportunity to manipulate its key properties, such as carrier density,[1,2] band structure,[3,4] and magnetism,[5] broadening its application in nanoelectronics.[6,7] Impurity atoms can be incorporated as either surface adatoms[8] or as dopants covalently bonded within the graphene lattice. Covalently bonded dopants in graphene are more robust and have been explored with a variety of elements, such as N,[9] Si,[10] Fe,[11,12] and Cu.[12] Several forms of impurity dopants have been studied from single atoms to larger 2D membranes containing hundreds of atoms. Robertson *et al.* reported the dynamics of single Fe atoms in monovacancies and divacancies, where nanoscale control of dopant incorporation was achieved by the use of controlled electron beam irradiation to create the initial vacancy that captures the mobile Fe atoms.[13] The single Fe dopants in graphene act as sites for trapping additional Fe atoms, leading to Fe dimer formation in graphene.[13] The Fe dimers were found to be mostly magnetic and offer a way of introducing magnetism into doped graphene.[14] Single Si dopants in graphene induce plasmonic enhancement, which may be important for future plasmonic devices.[15] The study of small clusters of impurity atoms in graphene has led to the direct observation of Si trimers and Si_6 clusters.[10,16] Under the electron beam, small clusters of Si atoms exhibit dynamics associated with structural reconfigurations, along with periods of fixed stability needed for image acquisition.[10,16] Monolayer 2D nanoscale regions containing tens and hundreds of Fe atoms suspended within graphene nanopores were recently observed.[17]

The introduction of impurity dopants into graphene with precise spatial control is challenging, and various methods have been explored, including chemical modification,[18,19] intercalation,[20,21] low-energy ion implantation,[22] and defect-assisted doping by electron beam irradiation.[13,14] The generation of vacancies or small holes in graphene from focused electron beam irradiation using an aberration-corrected transmission electron microscope (AC-TEM) at an accelerating voltage of 80 kV is a promising technique for the controlled introduction of dopants at the nanoscale.[23] The created defects exhibit enhanced chemical reactivity, which trap highly mobile adatoms residing on the graphene surface.[13] Silicon is one

* Address correspondence to jamie.warner@materials.ox.ac.uk.

Received for review June 8, 2015 and accepted July 20, 2015.

Published online July 24, 2015
10.1021/acsnano.5b03476

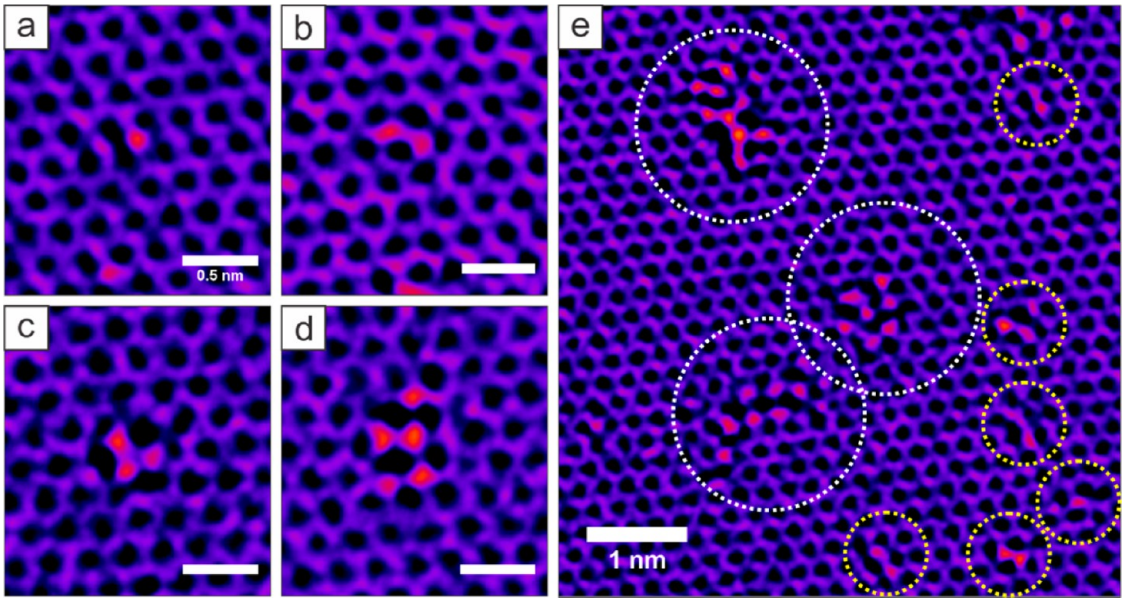

Figure 1. AC-TEM images showing examples of increasing cluster sizes of Si dopants in graphene ranging from (a) one, (b) two, (c) three, (d) five, and (e) a region of heavily doped graphene with multiple Si nanoclusters. White dashed circle indicates nanoclusters, and yellow dashed circle indicates atomic dopant and dimers.

of the most common dopants in synthetic graphene, arising from the quartz tubes used during chemical vapor deposition (CVD) growth, glass beakers, Si substrates, and Si_3N_4 TEM grids. The atomic structure and dynamics of both graphene and its individual dopants can be captured using AC-TEM, using low accelerating voltages of <80 kV.[24−26]

Prior atomic resolution studies of covalently bonded dopants in graphene using AC-TEM have focused primarily on either the very small clusters (1−6 atoms) or the larger 2D membranes, with little work undertaken on the intermediate size regime of small nanoclusters. For large numbers of atoms, crystalline periodic lattice structures will form, while in very small dopant clusters, such as trimers, there are not enough atoms present to form stable crystalline forms. In this report, we examine the atomic structure and time-dependent dynamics of Si nanoclusters that contain sufficient numbers of atoms to show the initial stages of periodic atomic ordering. The energy transferred from the electron beam to the graphene specimen can trigger the movement of impurity atoms, allowing time-dependent behavior to be studied.[13] Throughout the graphene sample, we observed several regions containing Si dopants covalently bonded in the lattice with cluster sizes ranging from 1 to 10, as shown in Figure 1. Energy-dispersive X-ray spectroscopy was measured from suspended regions of graphene containing patches of surface amorphous carbon that included heavier inorganic elements and were identified as Si (see Supporting Information Figure S1). Some areas contained a high density of Si dopants clusters with variable density, such as the area shown in Figure 1e, and within this area, we can locate several single Si atom dopants and dimers (yellow dashed circles) as well as Si nanoclusters with atomic numbers up to 10 or more (white dashed circles). The focus of this study is the structure of these Si nanoclusters and their dynamics.

RESULTS AND DISCUSSION

Under continuous electron beam irradiation at 80 kV, the small Si nanoclusters exhibit dynamic structural changes, but in many cases, they were stable enough in a cubic lattice configuration to obtain images with 2 s acquisition times. Figure 2i shows several examples from different regions of the sample, where Si nanoclusters adopt cubic arrangement of its atoms. A schematic atomic model of how the Si atoms can form such cubic arrangements is presented in Figure 2i,f. The cubic packing typically consists of pairs of Si atoms joined together to form anisotropic crystals, such as in Figure 2i,b. It is known that Si can adopt two different oxidation states when bonding in graphene, resulting in the connection to either three or four carbon atoms. Within the anisotropic crystals in Figure 2i, the Si atoms are all bonded to at least one C atom, and the Si atoms that are not at the ends of the crystal are bonded to three nearest neighbor Si atoms. Nonhexagonal carbon rings (*i.e.*, pentagons and heptagons) around the Si cluster cause deviation from exact symmetry in these structures. The anisotropic nanocrystals were stable for long enough to capture dynamics of the crystal lattice.

Figure 2ii shows the formation of an ordered Si cluster from a group of randomly located Si atoms. The Si atoms are restricted to a small area, as shown in Figure 2ii,a,b, and some Si atoms are even distorted (out-of-plane) due to the limited space in the graphene

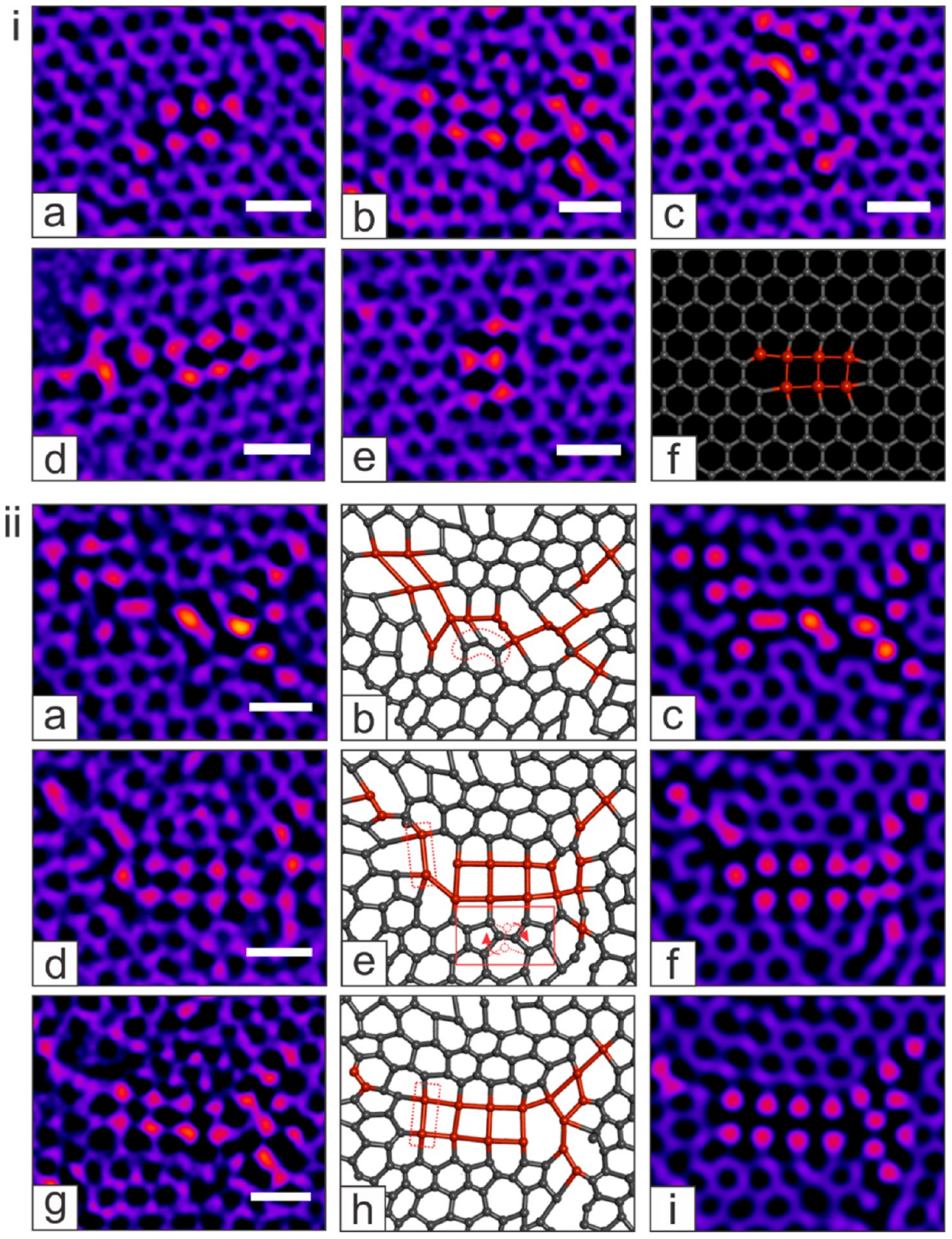

Figure 2. (i) (a–e) AC-TEM images of various Si clusters in graphene from different regions of the sample showing similar cubic structural forms. (f) Atomic model illustrating Si atoms covalently bonded in graphene adopting a cubic structure. (ii) (a) AC-TEM image of a Si cluster with randomly located Si atoms. (b) Atomic structural model for the AC-TEM image in (a); red atoms are for Si. (c) Multislice image simulation based on the atomic model in (b). (d) AC-TEM image of the same Si cluster in (a) but captured after 11 s. (e) Atomic structural model for the AC-TEM image in (d). (f) Multislice image simulation based on the atomic model in (e). (g) AC-TEM image taken 19 s after (d). (h) Atomic structural model for the AC-TEM image in (g). (i) Multislice image simulation based on the atomic model in (h). Red dotted closed curves in (ii,b) indicate the C atoms that are sputtered out. Scale bar: 0.5 nm.

lattice. This disordered Si cluster is unstable, and the rearrangement of Si atoms happens within 11 s. This restructuring is the consequence of the expansion of the local area, as three C atoms highlighted in Figure 2ii,b are sputtered out by electron beam irradiation. The sufficient space induces the formation of an

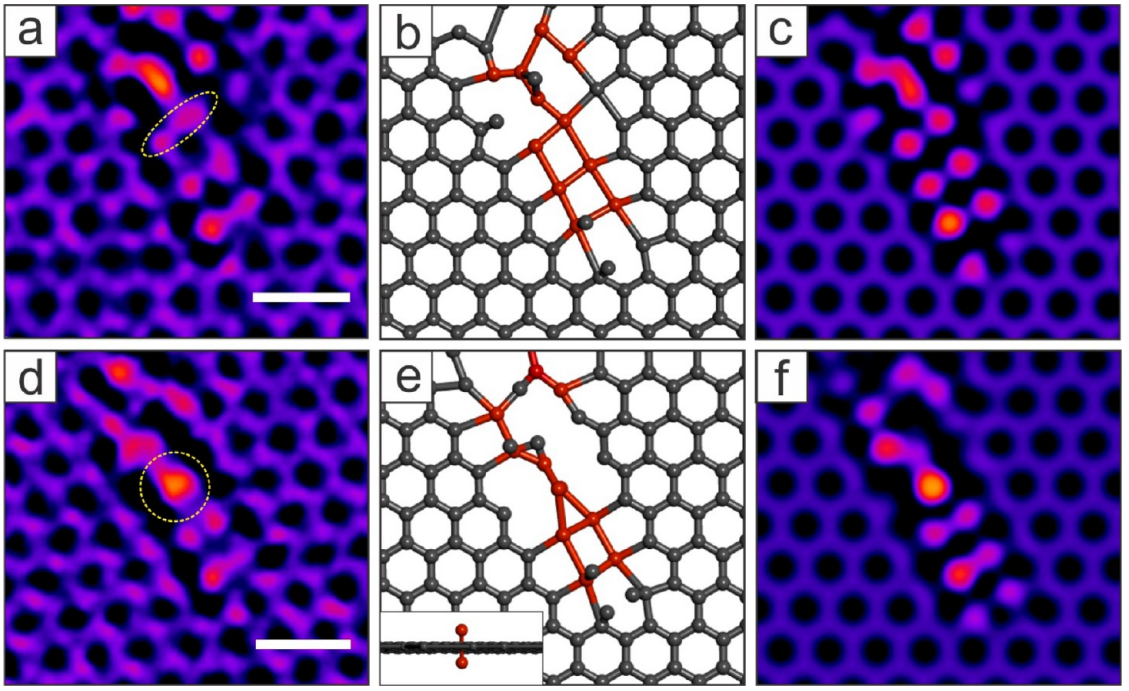

Figure 3. Ordered structure of a Si nanocluster and the out-of-plane rotation of two Si atoms. (a) Small Si nanocluster showing ordered cubic phases. The yellow dashed ellipse indicates the region where rotation occurs. (b) Atomic structural model for the AC-TEM image in (a). (c) Multislice image simulation based on the atomic model in (b). (d) Rotation of two Si atoms showing a vertically stacked structure, highlighted with a yellow dashed circle. The time duration between images in (d) and (a) is 8 s. (e) Atomic structural model for the AC-TEM image in (d), with the side view showing the vertically stacked Si atoms in the inset. (f) Multislice image simulation based on the atomic model in (e). Scale bar: 0.5 nm.

ordered Si cluster, shown in Figure 2ii,d. The C atoms connected to the Si cluster also adjust themselves to generate zigzag conformation. The two pentagons are likely generated from a bond rotation of the two C atoms along the zigzag edge, as shown in the red box in Figure 2ii,e, with the red dashed circles representing the positions of C atoms before bond rotation. The two Si atoms joining the existing ordered Si cluster is observed in Figure 2ii,d,g, and their atomic models (Figure 2ii,e,h show this more clearly.

The anisotropic Si nanoclusters could rotate such that two Si atoms were in projection. Figure 3 shows AC-TEM images of an ordered Si nanocluster (a,d) as well as the multislice image simulations (c,f) based on the atomic models (b,e). Two Si atoms (yellow dashed ellipse in Figure 3a rotated by 90°) form an out-of-plane structure (yellow dashed circle in Figure 3d) within 8 s. Box-averaged intensity profiles were taken from both the AC-TEM image and the simulation and confirm that the contrast matches well with the described out-of-plane rotated Si cluster (Figure S2 in Supporting Information). The evaluation method for distinguishing the different number of Si atoms in projection is the ratio of intensities: $(I_{\text{stacking Si}} - I_c)/(I_{\text{single Si}} - I_c)$. Subtracting the intensity of the carbon atom from both the vertically stacked Si pair and the single Si atom projections eliminates the influence of variable background levels. From the AC-TEM image, we obtained a value of 3.52, while for the simulated image, we obtained a value of 3.67, providing an excellent match. This confirms that the pair of Si atoms can rotate perpendicular to the graphene plane to form an out-of-plane structure with each Si atom located on either side of the graphene plane.

The dynamics of the Si atom rotation and local bonding changes are examined in Figure 4 (where Figure 3a,d is rotated clockwise by 37.5°, with bonds highlighted by lines for analysis purposes). A Klein edge, white dashed circle in Figure 4a, was initially observed and then disappeared by the next image in Figure 4b, and two additional C atoms (white circles) joined two pentagons to form hexagons. The additional C atoms may come from either the missing Klein edge or other highly mobile C adatoms. The rearrangement of C atoms indicates that the edge around the ordered Si cluster tends to adopt zigzag conformation, which consequently restricts the space of the two upper Si atoms. The two Si atoms rotate out-of-plane to compensate this shrinkage of space. The distance between the spots of contrast associated with Si–Si and Si–C bonds are measured to obtain more insights of before and after rotation.

The distances between two contrast spots from Si atoms before rotation are 2.05, 2.00, and 2.28 Å, but the actual Si–Si bond lengths may differ because a TEM image is a 2D projection of the 3D structure. To further explore the bond distances within the ordered cluster

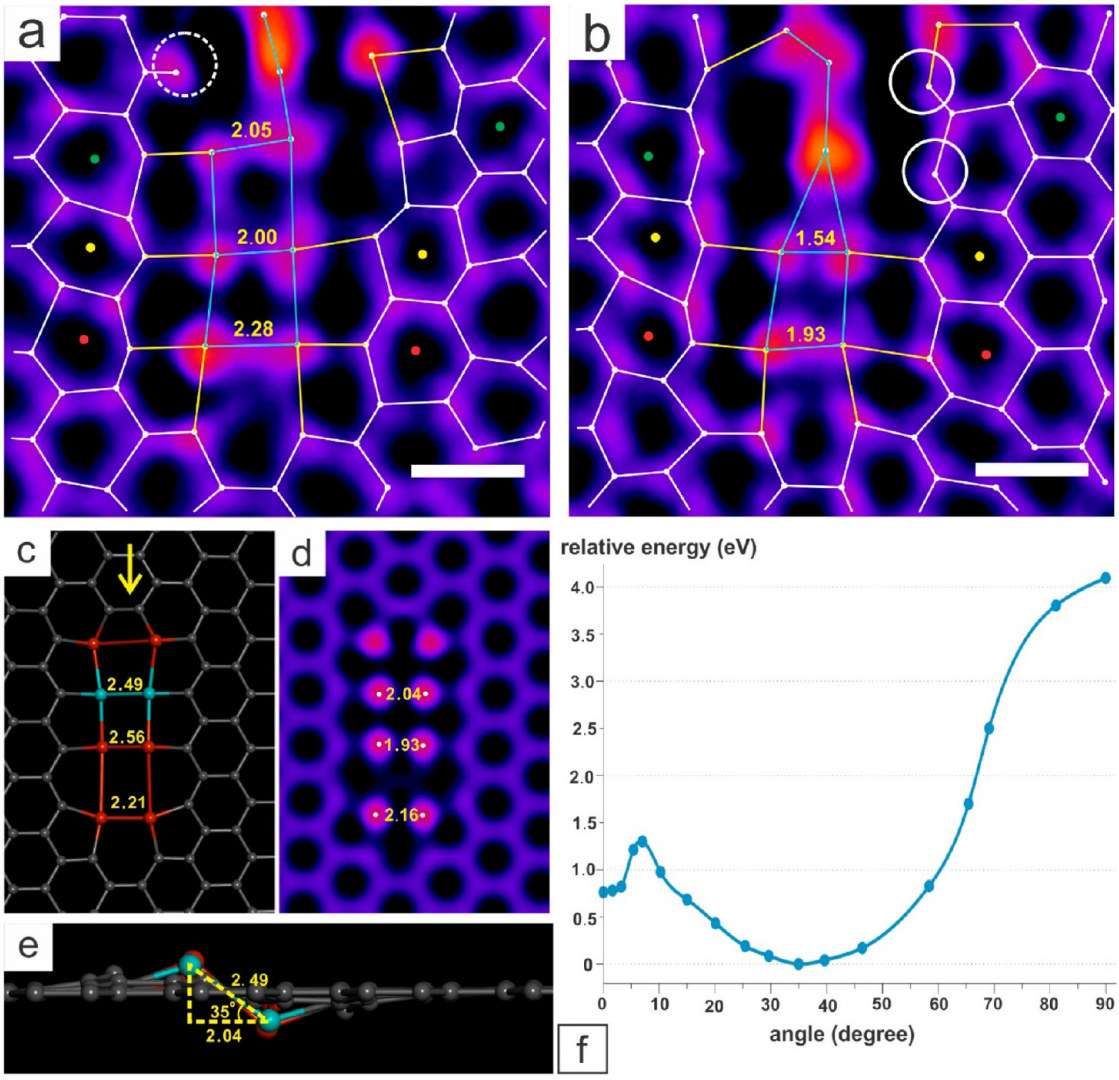

Figure 4. Bond lengths within an ordered Si cluster (a) before and (b) after rotation, with white lines for the C−C bond, yellow lines for the Si−C bond, and blue lines for the Si−Si bond. The white dashed circle in (a) shows a Klein edge that is missing in (b). The white circles in (b) show two additional C atoms contributing to form 6-atom rings. (c) DFT-calculated atomic model for a 6-atom ordered Si nanocluster (simplified from the model in Figure 3b) with calculated Si−Si bond lengths. (d) Multislice image simulation based on the atomic model in (c) with bond lengths determined using line profile measures from the image simulation. (e) Side view of (c) from the direction indicated by the yellow arrow. (f) Relative energy variation against the rotation angle of the highlighted Si pair in blue. The bond lengths are in angstroms. Scale bar: 3 Å.

when taking out-of-plane distortions into consideration, we utilized density functional theory (DFT) calculations. The fully relaxed atomic models from the DFT calculations have eliminated irrelevant carbon adatoms, as shown in Figure 4c, as well as used a Si pair (top) to represent the complex disordered Si atoms at the top of the crystalline Si cluster. The other six Si atoms adopt an ordered structure, with three horizontal Si−Si bonds of 2.49, 2.56, and 2.21 Å, from top to bottom, extracted from the DFT model, and the corresponding bond lengths measured from the multislice image simulations based on this model (Figure 4d) are 2.04, 1.93, and 2.16 Å. These measured bond distances show a good match with the experimental results. The difference between the real and projected bond lengths is mainly caused by the out-of-plane distortion of each Si−Si bond. The angle of the blue Si−Si bond is 35° (lateral view in Figure 4e), corresponding to the lowest point in the energy barrier plot (Figure 4f), indicating that the Si atoms in the ordered cluster are in the sp^3 rather than the sp^2d hybridization state, which forms a planar configuration.[27] When the angle increases to 90°, the two Si atoms stack vertically, as in Figures 3d and 4b, ~4 eV higher than the most stable state. This energy barrier is larger than the thermal contributions at room temperature but well within the energy transferred to the atoms by the electron beam for an accelerating voltage of 80 kV.

The graphene lattice surrounding the ordered Si cluster showed surprising stability with no measurable expansion or contraction after the Si atoms rotated. This is confirmed by measuring the lengths between

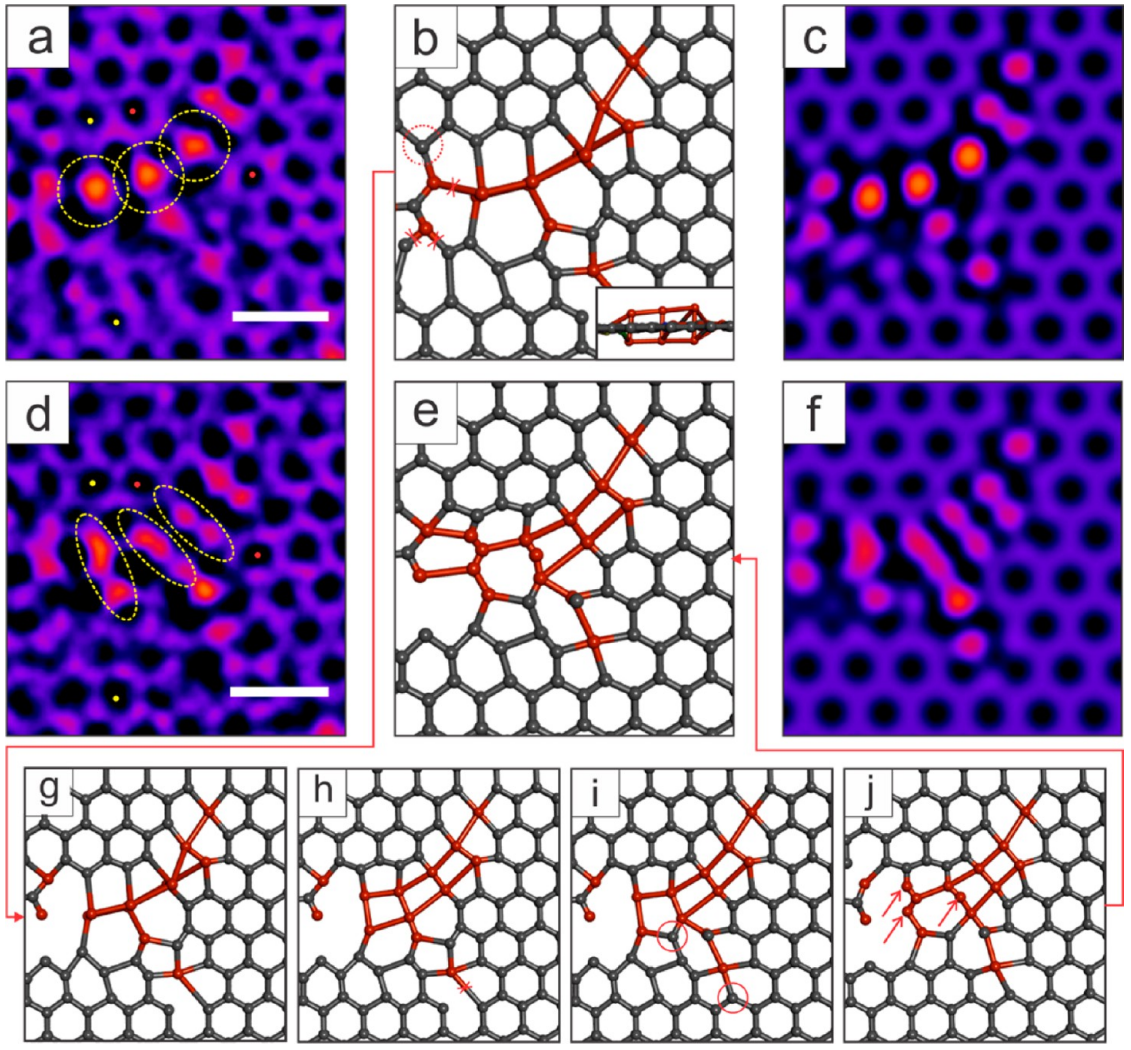

Figure 5. Si cluster showing the rotation of Si atoms. (a) AC-TEM images of a Si cluster, with the yellow dashed rings circling the stacking Si atoms. (b) Atomic structural model for the AC-TEM image in (a), with the inset showing the lateral view of the stacking structure. (c) Multislice image simulation based on the atomic model in (b). (d) AC-TEM image taken 10 s after (a). The yellow dashed ellipses highlight the rotated Si atoms. (e) Atomic structural model for the AC-TEM image in (d). (f) Multislice image simulation based on the atomic model in (d). (g–j) Pathway for the structure reconfiguration. Red dashed ring indicates the missing C atom in the following frame; red circle indicates the additional C atom; red arrows are for additional Si atoms, and crosses are for breaking bonds. Scale bar: 0.5 nm.

the centers of the 6-atom rings indicated with the same colored dots (red, yellow, and green), shown in Figure 4a,b. The distances between the red, yellow, and green spots are 0.85, 0.85, and 1.03 nm, respectively, both before and after the rotated Si atoms. These three values match the theoretical values for bulk graphene when no foreign atom is involved. It indicates that the pair of rotated stacked Si atoms is unlikely to be bonded to the neighboring C atoms as this covalent bond would cause structural distortions to the local graphene lattice. This is likely compensated by modified bonding to the neighboring Si atoms.

Figure 5 shows the opposite rotational behavior compared to Figures 3 and 4, where six Si atoms showing three out-of-plane stacking structures rotate to form two rows of crystalline structure within 10 s. The vertically stacked Si atoms, inset of Figure 5b, have three pairs of Si atoms perpendicular to the graphene lattice, confirmed by box-average intensity line profiles (see Supporting Information Figure S3). A plausible transformation pathway based on the two AC-TEM images is provided in Figure 5g–j. The change starts with a missing carbon atom bonded with a Si and two C atoms, highlighted by a red dashed circle in Figure 5b. The small cluster with two Si and a C atom shift upward to fill the vacancy, making the C atoms below rearrange to adopt a zigzag conformation (Figure 5g). This restructuring of Si and C atoms provides sufficient space for stacking atoms to relax (Figure 5h). The rotation may happen one-by-one from left to right. Figure 5i shows slight adjustment mainly on the migration of C atoms from elsewhere to form more stable structures, as highlighted by the red circles. The adjustment only takes place around relatively free Si atoms, whereas

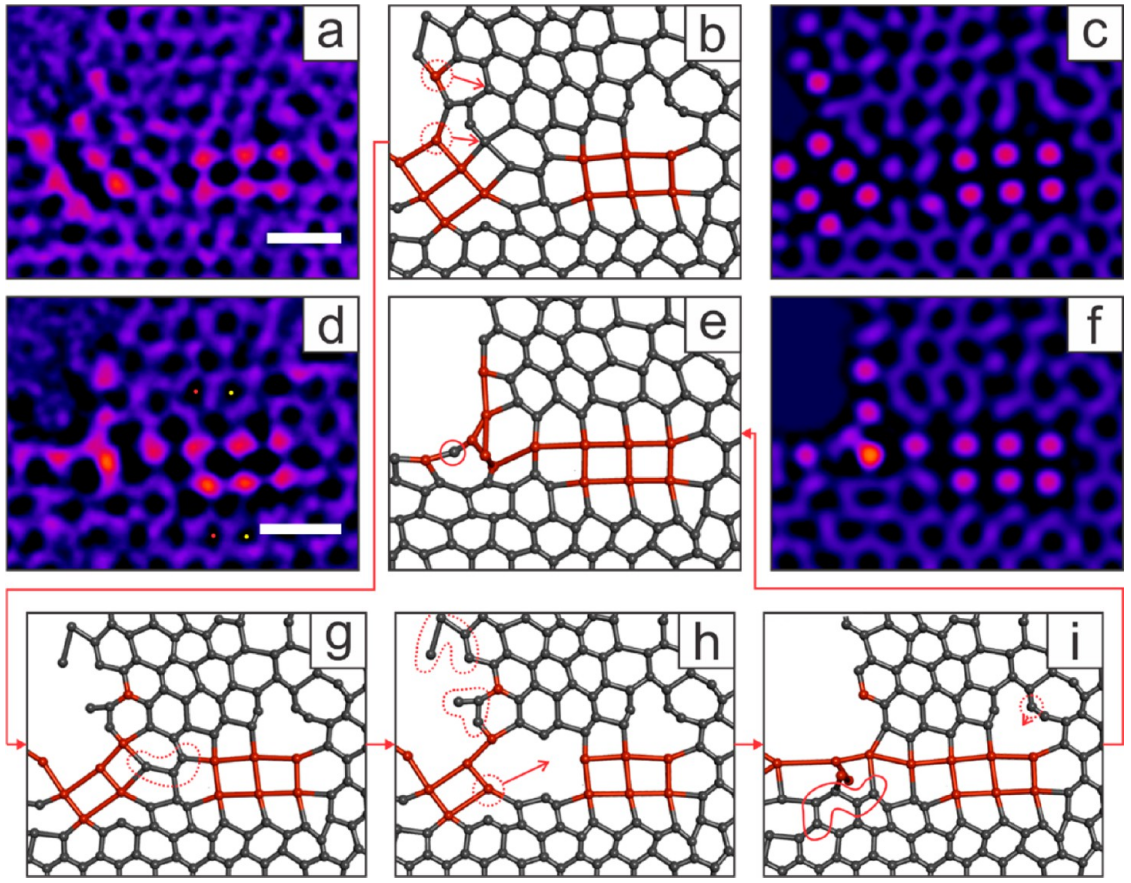

Figure 6. Dynamics of an ordered Si cluster next to a hole. (a) AC-TEM image of two ordered Si clusters, with the left one next to a hole and the right one further away in the graphene lattice. (b) Atomic structural model for the AC-TEM image in (a). (c) Multislice image simulation based on the atomic model in (b). (d) AC-TEM image taken 49 s after (a), showing the structural changes of the left Si cluster. (e) Atomic structural model for the AC-TEM image in (d). (f) Multislice image simulation based on the atomic model in (e). (g−i) Pathway for the structural reconfiguration. Atoms circled by red dashed closed curves are either sputtered out or moved to another region, and the ones inside the red solid closed curves are the additional atoms not present in previous images. Scale bar: 0.5 nm.

when the Si atoms bond to more C atoms in the graphene lattice, the structure is stable (for example, the three Si atoms at the top end of the Si cluster). Three additional Si atoms come into the Si cluster in Figure 5j (indicated by the red arrow). In this complicated Si cluster, most of the Si atoms are observed to have sp^3 hybridization, as well as some with three sp^2 bonds, and one bridge between two Si atoms forming a dangling bond.

This expansion of the Si cluster, involving stacked Si atoms relaxing as well as additional Si atoms joining in, does not influence the surrounding graphene structure. The distances between the same 6-atom rings (marked by red and yellow dots in Figure 5a,d) have the same values before and after the reshaping of the Si cluster. The length between the two 6-atom rings marked by red dots is 0.69 nm, and the two Si atoms between them are 0.15 nm apart after relaxation.

The behavior of an ordered Si cluster is affected by its location, especially when it is adjacent to a hole. Figure 6 provides a good example to compare the dynamics between two 6-atom Si clusters: one (left image in Figure 6a) is close to a hole, and the other one (right image in Figure 6a) is located in the bulk graphene lattice. It can be seen that after 49 s, the left Si cluster loses its ordered structure by atom rearrangement, while no obvious change is observed in the right Si cluster. The reshaping of the Si cluster adjacent to the hole is attributed to the higher mobility of edge atoms, meaning lower energy is required to displace them. A plausible pathway for the cluster restructuring is shown from Figure 6g−i. The hole is expanded due to the two Si atoms displacing the adjacent C atoms (Figure 6b,g), and the unstable dangling bonds and Klein edges are removed by continuous electron beam radiation (Figure 6h). Three C atoms between two Si clusters (red dotted region in Figure 6g) are also removed, due to the Si−C bond breaking. A Si atom moves into the vacancy left by the removed C atoms, combining with the larger existing ordered Si structure. Figure 6i shows five C atoms migrating into the lattice to form 6-atom rings, inducing the relocation of Si atoms. The additional C atoms probably come from the nearby sputtered C atoms, indicating that the

expansion of a hole is the combined effect of atomic elimination and reconstruction. The restructuring of C atoms also takes place at the boundary of the Si cluster and graphene lattice, as shown in Figure 6i. A C atom moves downward, contributing to the formation of complete zigzag edge. This agrees well with the findings in Figure 3 and Figure 4.

In comparison with the ordered 6-atom Si cluster in Figure 3a, the Si cluster (right) in Figure 6d has elongated bond lengths, as shown in Figure S4 in the Supporting Information. The average Si−Si bond length is 2.54 Å, which is longer than the theoretical value of the Si−Si bond in bulk. It indicates that the Si atoms are likely sitting planar in the graphene lattice without significant out-of-plane tilting. The graphene lattice around the Si cluster, as a consequence, is pushed away from its original location. The distances between the centers of the 6-atom rings highlighted by red and yellow dots in Figure 6d are 0.92 nm, which is nearly 10% longer than that in bulk graphene when no foreign atom is involved. The hole nearby the Si cluster probably contributes to the expanded structure, which is not observed in the former two Si clusters shown in Figure 3 and Figure 5, where both the Si clusters are located in the bulk graphene lattice. Therefore, when the surrounding graphene lattice is less rigid, the ordered Si cluster can adopt an in-plane structure.

The ordered Si clusters observed under the electron beam irradiation generally formed two rows, where each Si atom is connected to at least one C atom. Si atoms at the end of a row form sp^3 bonds with two C atoms and two Si atoms, while the ones at the middle section form sp^3 bonds with three Si atoms and a C atom. The reason why no Si atom with four Si neighbors is observed is attributed to the energy transferred from electron beam irradiation being higher than the threshold energy for knocking Si atoms with four adjacent Si atoms out of graphene lattice. Therefore, an ordered Si cluster with three or more rows is not able to stably exist under continuous electron beam irradiation at 80 kV accelerating voltage.

CONCLUSION

We show that crystalline anisotropic Si nanoclusters form the lattice of graphene and exhibit out-of-plane rotations under electron beam irradiation. These clusters contain 6−10 Si atoms, which line up in two rows to achieve stable Si−C bonds, suggesting that it is possible that longer embedded Si nanowire structures could be formed by extending the atomic number. The Si−C bonds within the nanoclusters tend to form along the zigzag direction of the graphene lattice. Switching between the vertically stacked Si atomic pair and the horizontal Si pair is likely driven by changes to the local space and atomic bonding, where restriction of space promotes the out-of-plane rotation and expansion of space encourages planar 2D Si clusters. Because the graphene is suspended in free space, access to both sides is available and we find that the vertically stacked Si pair can reside on either side of the lattice plane. This work demonstrates the complex crystalline structures that can be formed in-plane in graphene through strong covalent bonding to C atoms. Such nanoclusters are expected to be less mobile, compared to clusters that sit on top of the graphene lattice with weak van der Waals forces, and may open up new metal carbon systems for catalysis applications.

METHODS

Synthesis and Transfer of Graphene. Graphene was synthesized on the surface of a molten copper sheet, which acted as the catalyst, by CVD in atmospheric pressure using a previously reported method.[28] A 1 × 1 cm^2 high-purity copper foil (Alfa Aesar, Puratonic 99.999% purity) with a thickness of 0.1 mm was placed on the top of a tungsten sheet with the same size (Alfa Aesar, 99.95% purity, 0.05 mm thickness), positioned in a furnace, and then annealed at 1090 °C for 30 min with a mixture gas flow of 200 sccm pure argon and 100 sccm H_2 (20%)/Ar. To grow graphene, the H_2/Ar was then decreased to 80 sccm, with the addition of CH_4 (1%)/Ar to the system for 90 min. The sample was then cooled to room temperature under a H_2/Ar atmosphere. A poly(methyl methacrylate) (PMMA) supporting scaffold was coated on the graphene sample by spin-coating. The sample has a four-layer structure of tungsten/copper/graphene/PMMA from bottom to top. The tungsten layer was etched by an electrochemical reaction at 40 °C, with 2 mol/L NaOH solution as the electrolyte, tungsten as the anode, and a piece of copper foil (Alfa Aesar, 99.8% purity, annealed, 0.025 mm thickness) as the cathode, as previously reported.[29] The copper layer was then etched by 0.2 mol/L ammonium persulfate solution, leaving a graphene/PMMA film when finished. The film was then transferred to DI water several times to wash off any residual contamination from the etching process. The rinsed graphene/PMMA film was subsequently scooped up by a holey Si_3N_4 TEM grid (Agar Scientific Y5358), left to dry for 24 h, and then baked at 150 °C for 15 min to improve sample adhesion with the grid. Finally, the sample was heated in air at 350 °C overnight to remove the PMMA scaffold, leaving graphene on the TEM grid.

Transmission Electron Microscopy and Image Processing. Aberration-corrected TEM, along with energy-dispersive X-ray spectroscopy, was conducted using an FEI Titan 80-300 environmental TEM at 80 kV accelerating voltage. TEM images were processed using ImageJ. AC-TEM images were adjusted with a band-pass filter (between 100 and 1 pixels) to remove the long-range uneven illumination intensity and then smoothed using a Gaussian blur (3−5 pixels). Care was taken to ensure that this processing did not influence the interpretation of the original images. The original grayscale TEM images were taken with black atom contrast and then inverted, and a false color (fire) look-up table was used to improve the visual contrast. Atomic models based on the TEM images were generated using Accelrys Discovery Studio Visualizer, and multislice image simulations of the atomic models were generated using JEMS software with appropriate parameters set to match the conditions of the AC-TEM during imaging. The comprehensive experiment and analysis make it reliable for determination of the structures and time-dependent behavior of the ordered Si clusters.

Density Functional Theory Calculations. We performed DFT calculations within the generalized gradient approximation of the Perdew–Burke–Ernzerhof functional using the Vienna ab initio simulation package (VASP) code.[30,31] Vanderbilt pseudopotentials are also used in this calculation.[32] To make the unit cell containing Si atoms, 16 carbon atoms are pulled out from the supercell (21.38 Å × 32.08 Å × 30 Å) containing 240 carbon atoms and eight Si atoms are added. In the unit cell, the vacuum region of 30 Å is contained in the *z* direction. The basis set contains plane waves up to an energy cutoff of 400 eV. The Brillouin zone was sampled using a (3 × 2 × 1) Γ-centered mesh. When structural relaxations are performed, the angle of the Si dimer in the *xz* plane is fixed to calculate the rotation energy barrier of the Si dimer, and the structure is relaxed under the constraint until the force on each atom is smaller than 0.02 eV/Å.

Conflict of Interest: The authors declare no competing financial interest.

Supporting Information Available: EDX measurements of Si on graphene and measurements of atomic positions and bond lengths. The Supporting Information is available free of charge on the ACS Publications website at DOI: 10.1021/acsnano.5b03476.

Acknowledgment. J.H.W. thanks the Royal Society for support. Part of this work was performed at the Stanford Nano Shared Facilities (SNSF). G.D.L. acknowledges support from the Supercomputing Center/Korea Institute of Science and Technology Information with supercomputing resources (KSC-2014-C3-047) and from the National Research Foundation of Korea (NRF) grant funded by the Korea government (RIAM No. 2010-0012670).

REFERENCES AND NOTES

1. Bae, S.; Kim, H.; Lee, Y.; Xu, X.; Park, J.-S.; Zheng, Y.; Balakrishnan, J.; Lei, T.; Ri Kim, H.; Song, Y., Il; et al. Roll-to-Roll Production of 30-Inch Graphene Films for Transparent Electrodes. *Nat. Nanotechnol.* **2010**, *5*, 574–578.
2. Blake, P.; Brimicombe, P. D.; Nair, R. R.; Booth, T. J.; Jiang, D.; Schedin, F.; Ponomarenko, L. A.; Morozov, S. V.; Gleeson, H. F.; Hill, E. W.; et al. Graphene-Based Liquid Crystal Device. *Nano Lett.* **2008**, *8*, 1704–1708.
3. Zhou, S. Y.; Siegel, D. A.; Fedorov, A. V.; Lanzara, A. Metal to Insulator Transition in Epitaxial Graphene Induced by Molecular Doping. *Phys. Rev. Lett.* **2008**, *101*, 86402.
4. Elias, D. C.; Nair, R. R.; Mohiuddin, T. M. G.; Morozov, S. V.; Blake, P.; Halsall, M. P.; Ferrari, A. C.; Boukhvalov, D. W.; Katsnelson, M. I.; Geim, A. K.; et al. Control of Graphene's Properties by Reversible Hydrogenation: Evidence for Graphane. *Science* **2009**, *323*, 610–613.
5. Wang, Y.; Huang, Y.; Song, Y.; Zhang, X.; Ma, Y.; Liang, J.; Chen, Y. Room-Temperature Ferromagnetism of Graphene. *Nano Lett.* **2009**, *9*, 220–224.
6. Novoselov, K. S.; Fal'ko, V. I.; Colombo, L.; Gellert, P. R.; Schwab, M. G.; Kim, K. A Roadmap for Graphene. *Nature* **2012**, *490*, 192–200.
7. Arsat, R.; Breedon, M.; Shafiei, M.; Spizziri, P. G.; Gilje, S.; Kaner, R. B.; Kalantar-zadeh, K.; Wlodarski, W. Graphene-like Nano-Sheets for Surface Acoustic Wave Gas Sensor Applications. *Chem. Phys. Lett.* **2009**, *467*, 344–347.
8. Warner, J. H.; Rümmeli, M. H.; Bachmatiuk, A.; Wilson, M.; Büchner, B. Examining Co-Based Nanocrystals on Graphene Using Low-Voltage Aberration-Corrected Transmission Electron Microscopy. *ACS Nano* **2010**, *4*, 470–476.
9. Warner, J.; Lin, Y.; He, K.; Koshino, M.; Suenaga, K. Stability and Spectroscopy of Single Nitrogen Dopants in Graphene at Elevated Temperatures. *ACS Nano* **2014**, *8*, 11806–11815.
10. Yang, Z.; Yin, L.; Lee, J.; Ren, W.; Cheng, H.-M.; Ye, H.; Pantelides, S. T.; Pennycook, S. J.; Chisholm, M. F. Direct Observation of Atomic Dynamics and Silicon Doping at a Topological Defect in Graphene. *Angew. Chem., Int. Ed.* **2014**, *53*, 8908–8912.
11. Sevinçli, H.; Topsakal, M.; Durgun, E.; Ciraci, S. Electronic and Magnetic Properties of $3d$ Transition-Metal Atom Adsorbed Graphene and Graphene Nanoribbons. *Phys. Rev. B: Condens. Matter Mater. Phys.* **2008**, *77*, 195434.
12. Krasheninnikov, A. V.; Lehtinen, P. O.; Foster, A. S.; Pyykkö, P.; Nieminen, R. M. Embedding Transition-Metal Atoms in Graphene: Structure, Bonding, and Magnetism. *Phys. Rev. Lett.* **2009**, *102*, 126807.
13. Robertson, A. W.; Montanari, B.; He, K.; Kim, J.; Allen, C. S.; Wu, Y. A.; Olivier, J.; Neethling, J.; Harrison, N.; Kirkland, A. I.; et al. Dynamics of Single Fe Atoms in Graphene Vacancies. *Nano Lett.* **2013**, *13*, 1468–1475.
14. He, Z.; He, K.; Robertson, A. W.; Kirkland, A. I.; Kim, D.; Ihm, J.; Yoon, E.; Lee, G.-D.; Warner, J. H. Atomic Structure and Dynamics of Metal Dopant Pairs in Graphene. *Nano Lett.* **2014**, *14*, 3766–3772.
15. Zhou, W.; Lee, J.; Nanda, J.; Pantelides, S. T.; Pennycook, S. J.; Idrobo, J.-C. Atomically Localized Plasmon Enhancement in Monolayer Graphene. *Nat. Nanotechnol.* **2012**, *7*, 161–165.
16. Lee, J.; Zhou, W.; Pennycook, S. J.; Idrobo, J.-C.; Pantelides, S. T. Direct Visualization of Reversible Dynamics in a Si_6 Cluster Embedded in a Graphene Pore. *Nat. Commun.* **2013**, *4*, 1650.
17. Zhao, J.; Deng, Q.; Bachmatiuk, A.; Sandeep, G.; Popov, A.; Eckert, J.; Rümmeli, M. H. Free-Standing Single-Atom-Thick Iron Membranes Suspended in Graphene Pores. *Science* **2014**, *343*, 1228–1232.
18. Shi, Y.; Kim, K. K.; Reina, A.; Hofmann, M.; Li, L.-J.; Kong, J. Work Function Engineering of Graphene Electrode *via* Chemical Doping. *ACS Nano* **2010**, *4*, 2689–2694.
19. Farmer, D. B.; Golizadeh-Mojarad, R.; Perebeinos, V.; Lin, Y.-M.; Tulevski, G. S.; Tsang, J. C.; Avouris, P. Chemical Doping and Electron–Hole Conduction Asymmetry in Graphene Devices. *Nano Lett.* **2009**, *9*, 388–392.
20. Kim, N.; Kim, K. S.; Jung, N.; Brus, L.; Kim, P. Synthesis and Electrical Characterization of Magnetic Bilayer Graphene Intercalate. *Nano Lett.* **2011**, *11*, 860–865.
21. Zhan, D.; Sun, L.; Ni, Z. H.; Liu, L.; Fan, X. F.; Wang, Y.; Yu, T.; Lam, Y. M.; Huang, W.; Shen, Z. X. FeCl3-Based Few-Layer Graphene Intercalation Compounds: Single Linear Dispersion Electronic Band Structure and Strong Charge Transfer Doping. *Adv. Funct. Mater.* **2010**, *20*, 3504–3509.
22. Bangert, U.; Pierce, W.; Kepaptsoglou, D. M.; Ramasse, Q.; Zan, R.; Gass, M. H.; Van den Berg, J. A.; Boothroyd, C. B.; Amani, J.; Hofsäss, H. Ion Implantation of Graphene—Toward IC Compatible Technologies. *Nano Lett.* **2013**, *13*, 4902–4907.
23. Robertson, A. W.; Allen, C. S.; Wu, Y. A.; He, K.; Olivier, J.; Neethling, J.; Kirkland, A. I.; Warner, J. H. Spatial Control of Defect Creation in Graphene at the Nanoscale. *Nat. Commun.* **2012**, *3*, 1144.
24. Huang, P. Y.; Ruiz-Vargas, C. S.; van der Zande, A. M.; Whitney, W. S.; Levendorf, M. P.; Kevek, J. W.; Garg, S.; Alden, J. S.; Hustedt, C. J.; Zhu, Y.; et al. Grains and Grain Boundaries in Single-Layer Graphene Atomic Patchwork Quilts. *Nature* **2011**, *469*, 389–392.
25. Meyer, J. C.; Kisielowski, C.; Erni, R.; Rossell, M. D.; Crommie, M. F.; Zettl, a. Direct Imaging of Lattice Atoms and Topological Defects in Graphene Membranes. *Nano Lett.* **2008**, *8*, 3582–3586.
26. Robertson, A.; Warner, J. Atomic Resolution Imaging of Graphene by Transmission Electron Microscopy. *Nanoscale* **2013**, *5*, 4079–4093.
27. Zhou, W.; Kapetanakis, M. D.; Prange, M. P.; Pantelides, S. T.; Pennycook, S. J.; Idrobo, J.-C. Direct Determination of the Chemical Bonding of Individual Impurities in Graphene. *Phys. Rev. Lett.* **2012**, *109*, 206803.
28. Wu, Y. A.; Fan, Y.; Speller, S.; Creeth, G. L.; Sadowski, J. T.; He, K.; Robertson, A. W.; Allen, C. S.; Warner, J. H. Large Single Crystals of Graphene on Melted Copper Using Chemical Vapor Deposition. *ACS Nano* **2012**, *6*, 5010–5017.
29. Fan, Y.; He, K.; Tan, H.; Speller, S.; Warner, J. H. Crack-Free Growth and Transfer of Continuous Monolayer Graphene Grown on Melted Copper. *Chem. Mater.* **2014**, *26*, 4984–4991.

30. Perdew, J. P.; Burke, K.; Ernzerhof, M. Generalized Gradient Approximation Made Simple. *Phys. Rev. Lett.* **1996**, *77*, 3865–3868.
31. Kresse, G.; Furthmuller, J. Efficient Iterative Schemes for Ab Initio Total-Energy Calculations Using a Plane-Wave Basis Set. *Phys. Rev. B: Condens. Matter Mater. Phys.* **1996**, *54*, 11169–11186.
32. Vanderbilt, D. Soft Self-Consistent Pseudopotentials in a Generalized Eigenvalue Formalism. *Phys. Rev. B: Condens. Matter Mater. Phys.* **1990**, *41*, 7892–7895.